EPIGENETICS

MBD5 and MBD6 couple DNA methylation to gene silencing through the J-domain protein SILENZIO

Lucia Ichino[1,2], Brandon A. Boone[1,2], Luke Strauskulage[3,4], C. Jake Harris[2]†, Gundeep Kaur[5], Matthew A. Gladstone[2], Maverick Tan[2], Suhua Feng[2,6], Yasaman Jami-Alahmadi[7], Sascha H. Duttke[8], James A. Wohlschlegel[7], Xiaodong Cheng[5], Sy Redding[3], Steven E. Jacobsen[1,2,6,9]*

DNA methylation is associated with transcriptional repression of eukaryotic genes and transposons, but the downstream mechanism of gene silencing is largely unknown. Here, we describe two *Arabidopsis thaliana* methyl-CpG–binding domain proteins, MBD5 and MBD6, that are recruited to chromatin by recognition of CG methylation, and redundantly repress a subset of genes and transposons without affecting DNA methylation levels. These methyl readers recruit a J-domain protein, SILENZIO, that acts as a transcriptional repressor in loss-of-function and gain-of-function experiments. J-domain proteins often serve as co-chaperones with HSP70s. Indeed, we found that SILENZIO's conserved J-domain motif was required for its interaction with HSP70s and for its silencing function. These results uncover an unprecedented role of a molecular chaperone J-domain protein in gene silencing downstream of DNA methylation.

Cytosine DNA methylation (mC) in eukaryotes is typically associated with transcriptional silencing of genes and transposable elements (TEs); however, relatively little is known of the mechanism (*1*, *2*). Mammalian genomes encode for several methyl-CpG–binding domain (MBD) proteins that are recruited to chromatin in part by recognition of methylated CG dinucleotides, but they also play methylation-independent roles in gene regulation (*3*–*7*). One prevailing model is that MBDs recruit histone deacetylase complexes to methylated DNA, causing chromatin compaction and gene silencing (*5*–*7*). In plants, loss of DNA methylation causes derepression of many transposons and genes (*8*), but no evidence has been found for a role of methyl readers in this process, leaving unresolved the question of what acts downstream of the methyl mark.

We recently identified two proteins named MBD5 and MBD6 from a mass spectrometry screen for methyl readers in *Arabidopsis thaliana* (*9*). MBD5 and MBD6 belong to a family of 13 members that have been identified by sequence similarity with human MBD domains (*10*–*12*). Outside of this domain, there is no sequence conservation between plants and animals. MBD5 and MBD6 are close relatives (*10*–*12*), they can interact with each other in vivo (*13*, *14*), and were shown to bind methylated probes in electrophoretic mobility shift assays (*10*, *15*, *16*). Although a function has not been assigned to MBD5, MBD6 was shown to be required for ribosomal RNA gene regulation in allotetraploid genetic hybrids (*17*).

In plants, 5-methylcytosines are common in CG, CHG, and CHH sequence contexts (*18*). The MBD typically recognizes symmetrically methylated CG dinucleotides (*19*) but exceptions have been reported, for example, MeCP2, which can also bind mCA sites (*20*). We tested the ability of MBD5 and MBD6 to bind CG, CHG, or CHH methylation by performing fluorescence polarization (FP) assays with oligonucleotides methylated in different contexts. Both MBD5 and MBD6 showed a strong preference for CG-methylated oligonucleotides compared with unmethylated controls, but little preference was observed for CHG or CHH methylation (Fig. 1A and fig. S1). We also used DNA curtains, a single-molecule fluorescence microscopy assay, to visualize the interaction between MBD6 and flow-stretched bacteriophage λ DNA, which was methylated in vitro with the CG-specific bacterial *M.SssI* methyltransferase. MBD6 bound methylated, but not unmethylated, DNA curtains, and its enrichment profile correlated strongly with the local density of methylated CG sites (Fig. 1, B to D). To test the ability of MBD5 and MBD6 to bind methylation in natural *Arabidopsis* genomic sequences, we performed DNA affinity purification sequencing (DAP-seq) (*21*) by incubating Halo-tagged recombinant proteins with DNA extracted from wild-type plants or from *met1-3* mutant plants. The *met1-3* mutant is almost completely lacking in CG methylation because of a mutation in the maintenance *DNA METHYLTRANSFERASE 1* (*MET1*) gene but retains substantial levels of CHG and CHH methylation (*22*). We observed a strong genome-wide correlation between MBD5/6 DAP-seq enrichment and CG methylation density with DNA from a wild-type background and an almost complete loss of binding to DNA in the *met1-3* background (Fig. 1E). Only a few small peaks were retained in regions that did not completely lose CG methylation (fig. S2). Overall, these results strongly support the specificity of MBD5 and MBD6 for CG methylation in vitro.

We generated homology models of *Arabidopsis* MBD domains based on known mammalian MBD structures. High-confidence models could be determined except for the most divergent protein, MBD9, which is known not to bind methylated DNA in vivo (*23*) (fig. S3). The MBD5 and MBD6 structural models highlighted two arginine residues (R1 and R2) that are predicted to directly interact with methylated CGs by forming the previously described "methyl-Arg-G triad" (*19*) (Fig. 1F and fig. S3). We tested the importance of these residues by mutating them to alanine ($MBD5^{R1R2}$, $MBD6^{R1R2}$) and indeed we observed a loss of specificity for binding to CG methylation in FP assays (fig. S1B).

We next investigated the genomic localization of MBD5 and MBD6 in vivo by chromatin immunoprecipitation sequencing (ChIP-seq) using FLAG-tagged transgenic lines. MBD5 and MBD6 bound methylated chromatin with a clear preference for mCG density as opposed to mCHG and mCHH density (Fig. 1, G and H). No correlation was found with the density of unmethylated CG sites (fig. S4). The $MBD5^{R1R2}$ and $MBD6^{R1R2}$ mutants showed a strong reduction of ChIP-seq enrichment (Fig. 1G and fig. S5), demonstrating that recognition of mCGs is required for recruitment of MBD5 and MBD6 to chromatin.

Methylated DNA is associated with three different chromatin states in *Arabidopsis*: euchromatic patches of RNA-directed DNA methylation (RdDM), which contain CG and non-CG methylation; pericentromeric heterochromatin, which is enriched in H3K9me2 as well as CG and non-CG methylation; and expressed genes containing gene body methylation (GbM), which are exclusively marked by CG methylation (*18*). We observed MBD5 and MBD6 ChIP-seq enrichment at a large fraction of sites in all three chromatin states, but the extent of enrichment was higher at RdDM sites compared with heterochromatin or GbM sites (fig. S6). However, the preference for RdDM sites was not observed by DAP-seq, which tests the ability of proteins to bind naked genomic DNA (fig. S6, C and D).

[1]Molecular Biology Institute, University of California Los Angeles, Los Angeles, CA 90095, USA. [2]Department of Molecular, Cell and Developmental Biology, University of California Los Angeles, Los Angeles, CA 90095, USA. [3]Department of Biochemistry and Biophysics, University of California San Francisco, San Francisco, CA 94143, USA. [4]Tetrad Graduate Program, University of California San Francisco, San Francisco, CA 94143, USA. [5]Department of Epigenetics and Molecular Carcinogenesis, University of Texas MD Anderson Cancer Center, Houston, TX 77030, USA. [6]Eli and Edyth Broad Center of Regenerative Medicine and Stem Cell Research, University of California Los Angeles, Los Angeles, CA 90095, USA. [7]Department of Biological Chemistry, University of California Los Angeles, Los Angeles, CA 90095, USA. [8]Department of Medicine, University of California San Diego, La Jolla, CA 92093, USA. [9]Howard Hughes Medical Institute (HHMI), University of California Los Angeles, Los Angeles, CA 90095, USA.
*Corresponding author. Email: jacobsen@ucla.edu
†Present address: Department of Plant Sciences, University of Cambridge, Cambridge CB2 3EA, UK.

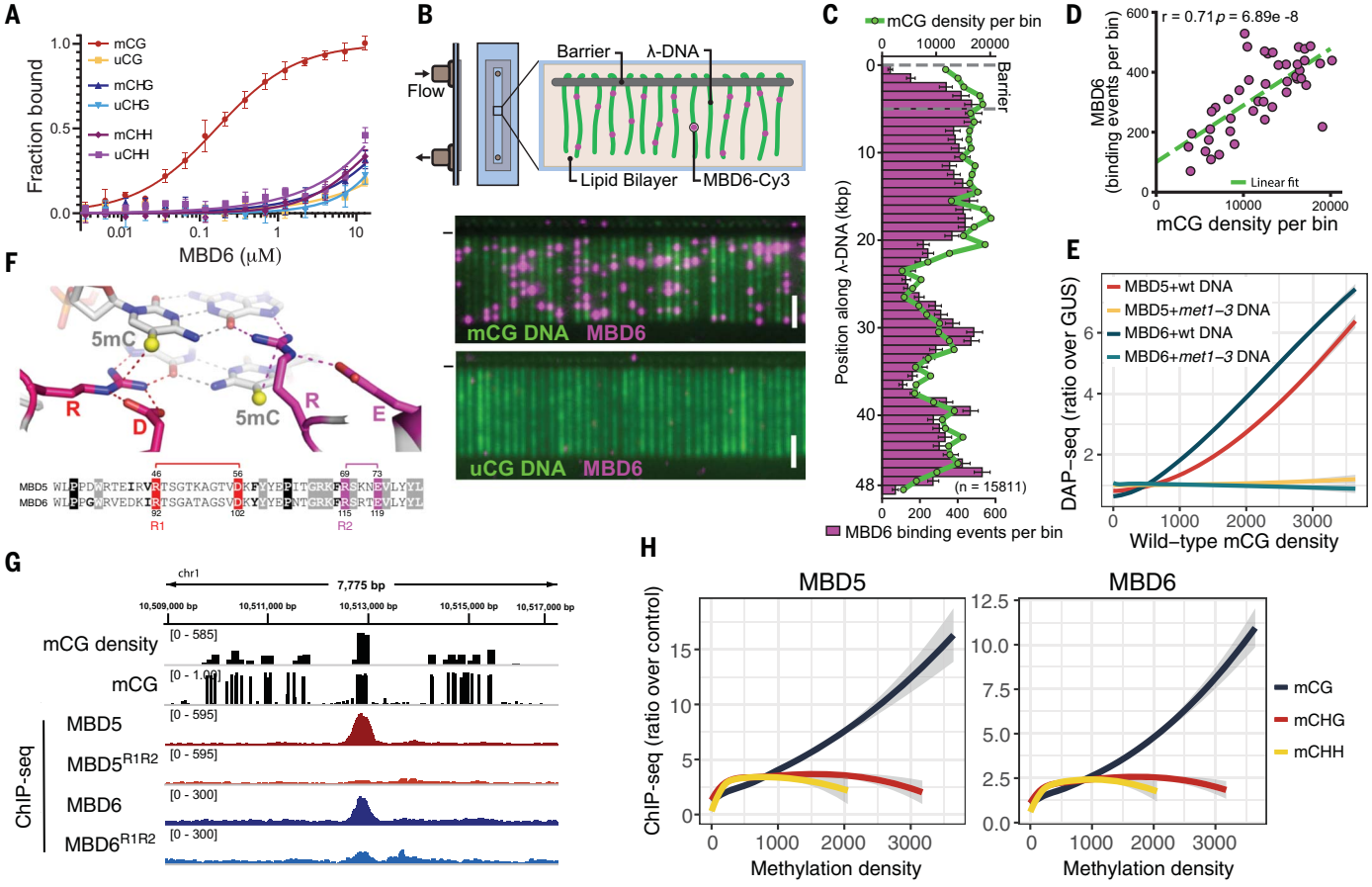

Fig. 1. MBD5 and MBD6 are CG-specific methyl readers in vitro and in vivo. (**A**) Binding curves of MBD6 with DNA oligos methylated (m) or unmethylated (u) in the indicated contexts, measured by fluorescence polarization (N = 3, SEM). (**B**) Diagram of DNA curtain assay and representative image of YOYO-1–stained methylated (mCG) and unmethylated (uCG) DNA (green) bound by Cy3-labeled MBD6 (magenta). Horizontal lines on the lower panels indicate the chrome diffusion barriers. Scale bars, 5 μm. (**C**) Distribution of MBD6-binding events along mCG DNA overlaid with the distribution of mCG density (green line). Error bars indicate the 95% confidence intervals (CI) by bootstrap. (**D**) Correlation scatterplot of MBD6 binding to methylated curtains and mCG density (1-kb bins). r is the Pearson correlation coefficient. (**E**) Genome-wide correlation between DAP-seq and mCG density (400-bp bins). Trend lines were calculated by locally weighted polynomial regression (loess curves). (**F**) Homology models of MBD5 and MBD6. The two arginine residues of the 5mC–Arg–G triads (R1 and R2) are shown in the sequence alignment. (**G**) Example ChIP-seq peaks at regions of dense CG methylation. (**H**) Loess curves of ChIP-seq enrichment and methylation density (400-bp bins overlapping Pol V ChIP-seq peaks). For (E) and (H), shaded area indicates 95% CI.

These observations suggest that recruitment of MBD5 and MBD6 to chromatin in vivo may be influenced by histones or other chromatin components.

To determine whether MBD5 and MBD6 regulate transcription at their targets, we performed RNA sequencing (RNA-seq) of *mbd5* and *mbd6* T-DNA mutants and of a double mutant generated by crossing them (*mbd5 mbd6*). A number of transposons and protein-coding genes were derepressed only in the double mutant, indicating genetic redundancy of *MBD5* and *MBD6* (Fig. 2A and fig. S7). We confirmed this with an independent *mbd5 mbd6* double mutant generated by CRISPR/Cas9 (figs. S7 and S8). Global run-on sequencing (GRO-seq) showed a similar pattern of changes, indicating that the derepression in *mbd5 mbd6* occurs at the transcriptional level (Fig. 2B). Most up-regulated genes and transposons were not expressed in wild-type plants and showed high levels of promoter CG methylation, suggesting that they are direct targets (Fig. 2C). DNA methylation levels were not altered in *mbd5 mbd6* (Fig. 2C and fig. S9), indicating that the methyl readers act strictly downstream of DNA methylation. One of the derepressed genes was *FWA*, a well-characterized imprinted gene that is silenced by promoter methylation (*24*) (Fig. 2, D and E). Reintroduction into *mbd5 mbd6* mutant plants of FLAG-tagged versions of wild-type MBD5 or MBD6, but not their R1R2 mutant counterparts, was sufficient to largely rescue the derepression of *FWA* and of other genes and transposons (fig. S10). Overall, these results suggest that MBD5 and MBD6 are recruited to DNA by methylation and translate the methyl mark into gene repression at a subset of methylated sites.

We compared *mbd5 mbd6* gene expression data with those of mutants affecting different methylation pathways: *drm1 drm2* and *cmt2 cmt3* lose non-CG methylation at euchromatic RdDM sites and heterochromatic regions, respectively, whereas *met1-3* loses CG methylation genome-wide (*22*, *25*). Most of the loci up-regulated in *mbd5 mbd6* were also derepressed in *met1-3*, indicating that they are silenced by CG methylation (fig. S11A). TEs derepressed in *mbd5 mbd6* were also longer than average and more enriched in H3K9me2, indicating that they are mostly heterochromatic TEs (fig. S11, B and C). A subset of these loci were also derepressed in *cmt2 cmt3*, but there were none derepressed in *drm1 drm2* (fig. S11A). Thus, whereas MBD5 and MBD6 are enriched at a wide range of CG-methylated sites, their repressive role is strongest at a subset of MET1-dependent heterochromatic loci. Furthermore,

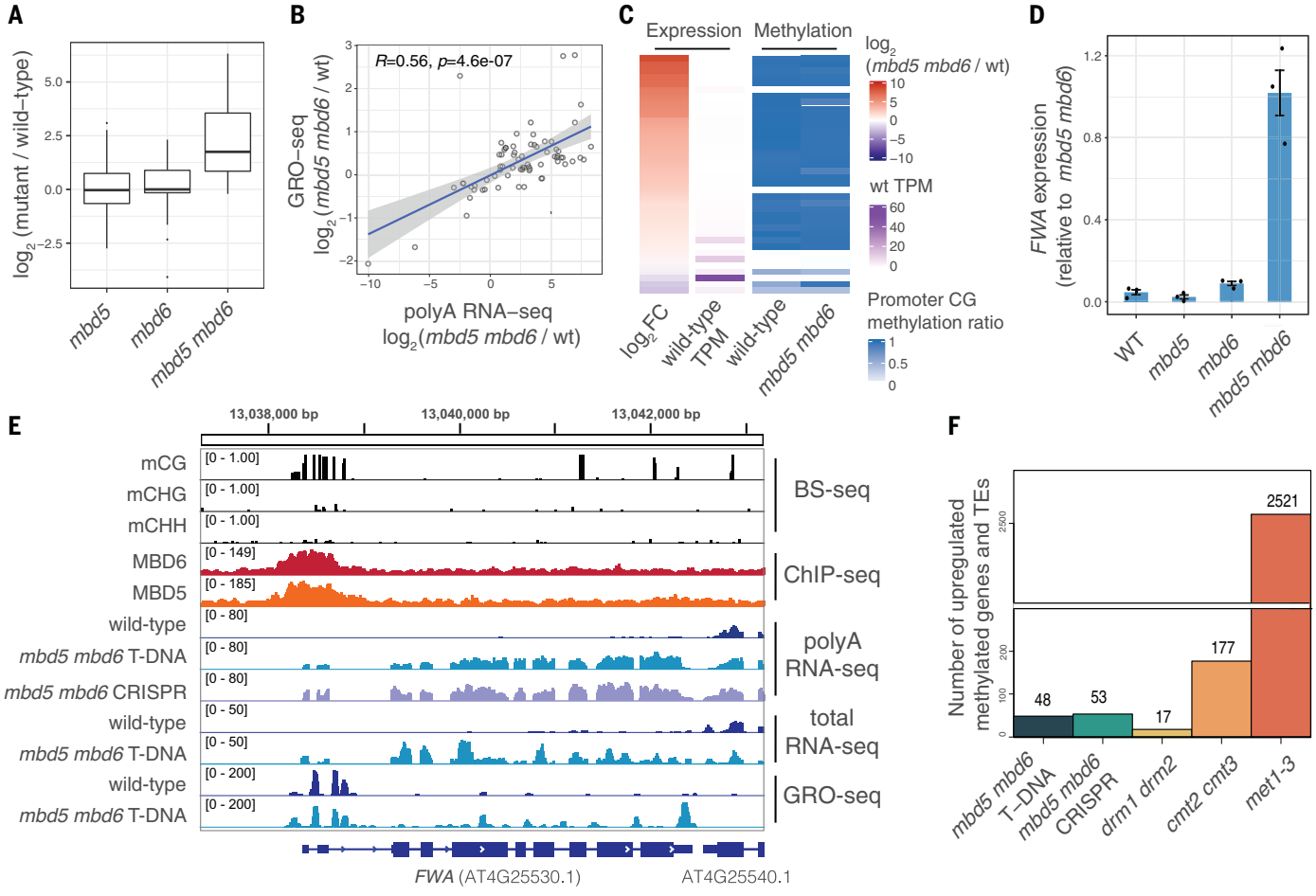

Fig. 2. MBD5 and MBD6 redundantly repress a subset of genes and transposons downstream of DNA methylation. (**A**) Boxplot of poly(A) RNA-seq for different mutants. Shown are the transcripts (genes and transposons) up-regulated in *mbd5 mbd6*. (**B**) Scatterplot comparing poly(A) RNA-seq with GRO-seq data at *mbd5 mbd6* T-DNA differential transcripts. *R* is the Spearman's rank correlation coefficient and *p* is the *P* value of the test that *R* = 0. Shaded area indicates 95% CI. (**C**) Heatmap of *mbd5 mbd6* T-DNA differential transcripts showing poly(A) RNA-seq and BS-seq data (average methylation ratio at 400-bp windows around the TSS). (**D**) Reverse transcription quantitative polymerase chain reaction (RT-qPCR) analysis of *FWA* expression normalized to *IPP2*. Dots indicate individual plants. Error bars indicate SEM. (**E**) Genome browser tracks at *FWA*. The GRO-seq enrichment at the *FWA* promoter likely corresponds to Pol V transcription. (**F**) Number of promoter methylated genes and TEs that are up-regulated in different mutants.

the number of derepressed transposons and the amplitude of derepression in *mbd5 mbd6* was much smaller than in *met1-3* (Fig. 2F and fig. S11), suggesting that MBD5 and MBD6 are not the only factors mediating repression downstream of DNA methylation.

To investigate the mechanism of action of MBD5 and MBD6, we performed immunoprecipitation–mass spectrometry (IP-MS) using the FLAG-tagged transgenic lines. Both proteins pulled down each other and three small heat shock proteins (ACD15.5, ACD21.4, and IDM3/LIL) that were previously found to interact with MBD5 and MBD7 (*13*). In addition, we detected an uncharacterized class C J-domain protein (AT5G37380) (*26*, *27*) that we have named SILENZIO (SLN) (Fig. 3A and table S1). MBD5 and MBD6 also pulled down a smaller number of peptides of SUVH1, SUVH3, DNAJ1, and DNAJ2, which are components of a methyl-reader complex known to bind at RdDM sites and up-regulate nearby protein-coding genes (*9*, *28*).

We focused our further investigation on SILENZIO because of the recently described role of the J-domain proteins DNAJ1 and DNAJ2 in gene activation downstream of DNA methylation (*9*, *28*). SILENZIO homologs were found to be present widely throughout the plant kingdom, but only the J-domain was conserved in animals (fig. S12). To determine whether SILENZIO was involved in gene silencing, we performed RNA-seq on an *sln* T-DNA mutant line. We found a strong correlation between the *sln* and the *mbd5 mbd6* RNA-seq data, with a similar extent of derepression of TEs and genes, including *FWA* (Fig. 3, B and C). We performed ChIP-seq with a complementing FLAG-tagged SLN line (fig. S13) and observed localization to the same sites as MBD5 and MBD6, but this localization was abolished in *mbd5 mbd6* mutants, suggesting that SLN is recruited to chromatin by the methyl readers (Fig. 3, D and E, and fig. S14). Conversely, the MBD5 and MBD6 ChIP-seq signals were unaffected in *sln*, indicating that their recruitment to chromatin does not require SLN (Fig. 3, D and E, and fig. S14). Overall, these results suggest that SLN acts as a gene repressor downstream of MBD5 and MBD6.

To further test the role of SLN as a repressor, we created a fusion of SLN with ZF108, an artificial zinc finger that allows ectopic targeting of proteins to the *FWA* promoter (Fig. 3F) (*29*, *30*). We transformed this fusion construct driven by the constitutive *UBIQUITIN10* promoter (*pUBQ10::ZF108-SLN*) into *fwa* epi-allele mutant plants (*24*) in which the *FWA* gene has heritably lost DNA methylation, leading to *FWA* overexpression and a late-flowering phenotype. Transgenic (T1) plants that expressed high levels of the fusion protein displayed down-regulation of *FWA*, thus supporting a role of

A

ID	Protein	MBD5 rep1	MBD5 rep2	MBD6 rep1	MBD6 rep2
AT3G46580	MBD5	160	151	56	39
AT5G59380	MBD6	51	72	168	244
AT5G37380	SLN	23	28	29	21
AT1G76440	ACD15.5	71	58	38	53
AT1G54850	ACD21.4	87	80	40	62
AT1G20870	IDM3/LIL	9	0	44	101
AT5G04940	SUVH1	21	11	9	11
AT1G73100	SUVH3	2	5	3	0
AT5G64360	DNAJ1	4	2	5	0
AT2G01710	DNAJ2	10	7	10	8

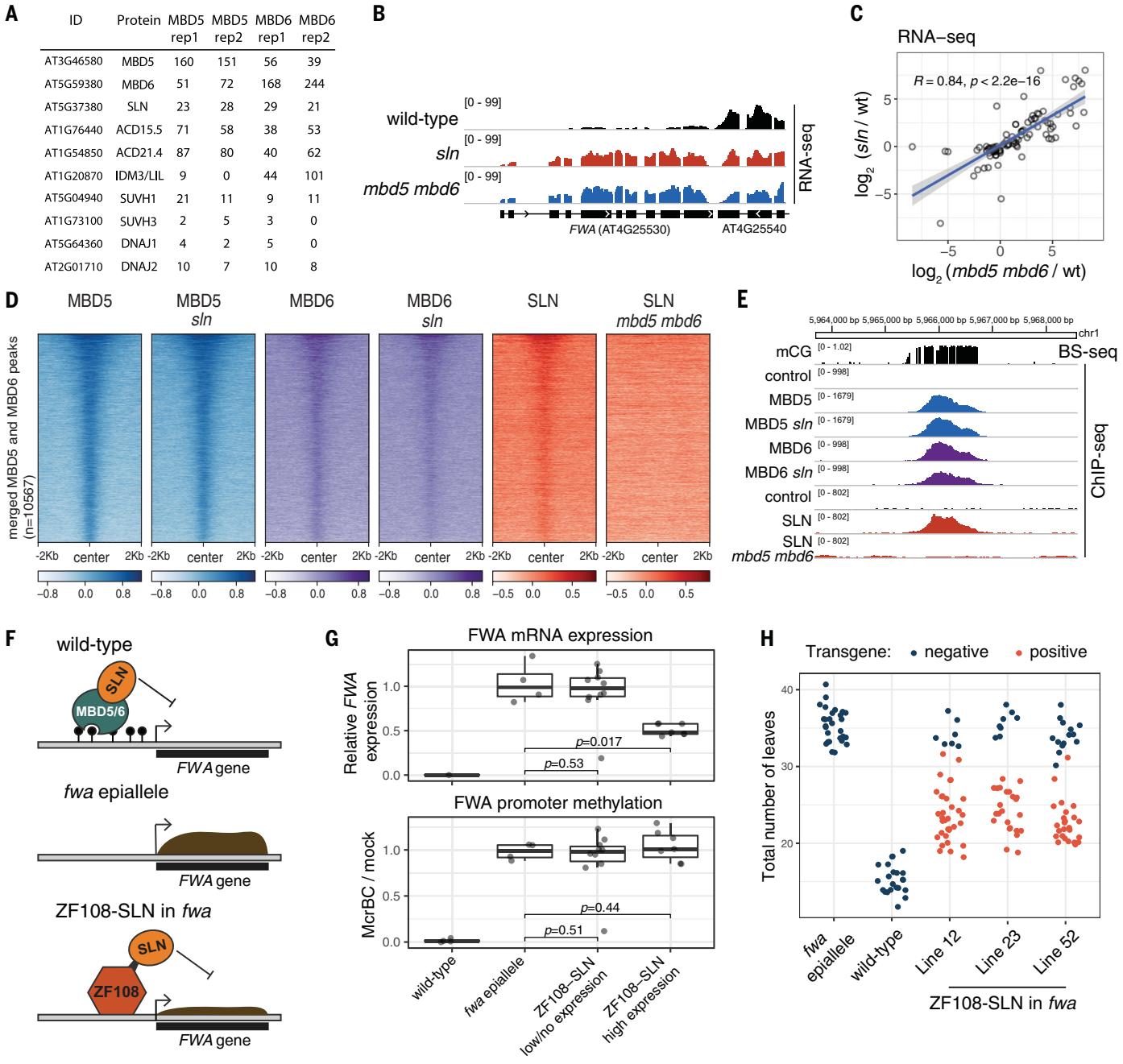

Fig. 3. SLN represses transcription downstream of MBD5 and MBD6. (**A**) Spectral counts of proteins detected by IP-MS of FLAG-tagged MBD5 and MBD6. All proteins displayed were not detected in the no-FLAG negative control (see table S1). (**B**) RNA-seq data at *FWA*. (**C**) Scatterplot of the union of *mbd5 mbd6* CRISPR and *sln* differential transcripts. *R* is the Spearman's rank correlation coefficient and *p* is the *P* value of the test that *R* = 0. Blue line indicates the linear model fit. Shaded area indicates 95% CI. (**D**) Heatmap of ChIP-seq data (log_2-fold change over the no-FLAG control). (**E**) Example methylated site bound by MBD5, MBD6, and SLN in the indicated backgrounds. (**F**) Diagram showing SLN's ectopic recruitment to unmethylated *FWA* through fusion to ZF108. (**G**) RT-qPCR analysis of *FWA* expression and McrBC-qPCR analysis of *FWA* promoter methylation in T1 lines expressing low or high levels of ZF108-SLN (Western blot in fig. S15A). Dots indicate individual plants. *p* is the *P* value of the Student's *t* test for each pair of groups. RT-qPCR data (normalized to *IPP2*) are relative to *fwa* epi-allele plants. (**H**) Flowering time (number of leaves produced before flowering) of segregating T2 populations from three transgenic lines expressing high levels of ZF108-SLN, comparing transgene-positive with null segregant (negative) plants.

SLN as transcriptional repressor (Fig. 3G and fig. S15A). *FWA* repression was not accompanied by promoter methylation (Fig. 3G and fig. S15B), demonstrating that SLN's ability to repress transcription can be uncoupled from DNA methylation. Indeed, in the T2 segregant population, the null segregants recovered *FWA* overexpression and the corresponding late flowering time (Fig. 3H and fig. S15C). ZF108 was designed to bind *FWA*, but it also binds to thousands of off-target sites in the genome (*30*), allowing us to examine gene expression changes at these sites by performing RNA-seq in the *pUBQ10::ZF108-SLN* lines. We observed that genes with a ZF108 peak near their

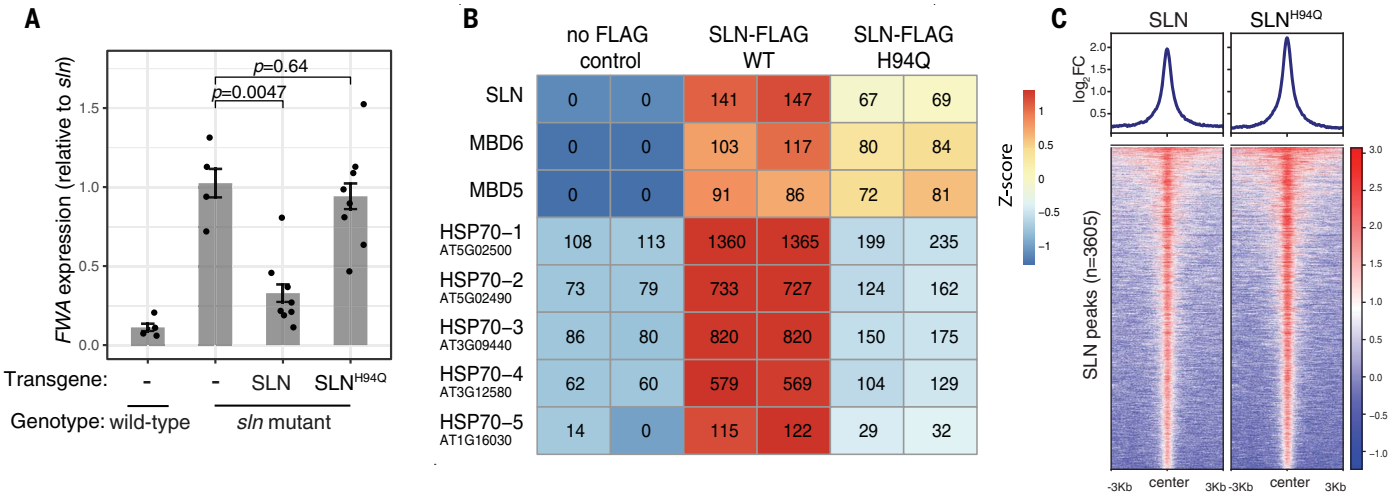

Fig. 4. SLN-silencing function requires the conserved HPD tripeptide. (**A**) RT-qPCR analysis of *FWA* expression (normalized to *IPP2*) in T1 lines expressing SLN or SLN^{H94Q} in the *sln* mutant background. *p* is the *P* value of the Student's *t* test for each pair of groups. Error bars indicate SEM. Dots indicate individual plants. (**B**) Spectral counts of proteins detected by IP-MS of wild-type and H94Q mutant SLN-FLAG (representative of two independent experiments; see table S1). (**C**) ChIP-seq of FLAG-tagged SLN and SLN^{H94Q} (log_2-fold change over the no-FLAG control).

promoter showed a tendency to be down-regulated (fig. S16), demonstrating that ectopic recruitment of SLN can repress many genes in addition to *FWA*.

IP-MS analysis of SLN-FLAG identified peptides corresponding to MBD5 and MBD6, as expected, but also showed a strong enrichment of five HEAT SHOCK PROTEIN 70 (HSP70) chaperones known to be constitutively expressed and localized in the nucleus (*31*) (Fig. 4B and table S1). Enrichment for HSP70s was also detected in the MBD5 and MBD6 IP-MS datasets and was lost in *sln* mutant plants (fig. S17 and table S1). This suggests that SLN mediates the interaction between the methyl readers and the HSP70s.

The canonical function of J-domain proteins is to bind clients, recruit HSP70 chaperones using a conserved HPD tripeptide, and stimulate the ATPase activity of HSP70s to increase their affinity for substrates. The HSP70-substrate interaction can induce folding, disaggregation, assembly, or disassembly of complexes involving client proteins (*32*). Mutating the histidine of the HPD tripeptide to glutamine can abrogate the J-domain–HSP70 interaction (*32*). To test whether SLN's binding to HSP70s was associated with its gene-silencing function, we generated an HPD mutant version of SLN by mutating the histidine to glutamine (SLN^{H94Q}) and transformed this into *sln* mutant plants. The SLN^{H94Q} mutant failed to rescue the derepression of *FWA* and of the other genes and transposons, suggesting that the gene-silencing function of SLN requires the J-domain and HSP70 interaction (Fig. 4A and fig. S18, A to F). Indeed, IP-MS of SLN^{H94Q} showed greatly reduced enrichment of HSP70s, whereas the interaction with MBD5 and MBD6 was retained (Fig. 4B and table S1). Furthermore, ChIP-seq enrichment of SLN on chromatin was not affected by the H94Q mutation (Fig. 4C and fig. S18, G and H). These results suggest that recruitment of SLN by the methyl readers may serve as a tether to bring the chaperone activity of SLN-HSP70s to CG-dense methylated chromatin to enforce gene silencing. The interaction between chaperones and their clients is often transient and difficult to detect by IP-MS (*32*), meaning that SLN might exert its repressive activity through recruitment, stabilization, or assembly of currently unknown repressive complexes or by targeted inhibition or disassembly of activators.

In conclusion, this work identifies a pathway that links DNA methylation to silencing of sites marked by CG methylation. The characterization of the methyl-binding proteins MBD5 and MBD6 shows that they likely act through a mechanism distinct from that of known MBD proteins in animals. The identification of the J-domain protein SILENZIO as a silencing effector further suggests that gene repression downstream of methylation is linked to chaperone activity, and this new pathway is likely to be conserved among divergent plant lineages.

REFERENCES AND NOTES

1. M. G. Goll, T. H. Bestor, *Annu. Rev. Biochem.* **74**, 481–514 (2005).
2. A. Zemach, I. E. McDaniel, P. Silva, D. Zilberman, *Science* **328**, 916–919 (2010).
3. T. Baubec, R. Ivánek, F. Lienert, D. Schübeler, *Cell* **153**, 480–492 (2013).
4. T. Shimbo, P. A. Wade, *Adv. Exp. Med. Biol.* **945**, 303–320 (2016).
5. L. D. Boxer *et al.*, *Mol. Cell* **77**, 294–309.e9 (2020).
6. M. J. Lyst *et al.*, *Nat. Neurosci.* **16**, 898–902 (2013).
7. X. Nan *et al.*, *Nature* **393**, 386–389 (1998).
8. X. Zhang *et al.*, *Cell* **126**, 1189–1201 (2006).
9. C. J. Harris *et al.*, *Science* **362**, 1182–1186 (2018).
10. A. Zemach, G. Grafi, *Plant J.* **34**, 565–572 (2003).
11. A. Berg *et al.*, *Nucleic Acids Res.* **31**, 5291–5304 (2003).
12. N. M. Springer, S. M. Kaeppler, *Plant Physiol.* **138**, 92–104 (2005).
13. D. Li *et al.*, *eLife* **6**, e19893 (2017).
14. A. Zemach *et al.*, *Plant Cell* **17**, 1549–1558 (2005).
15. F. Scebba *et al.*, *Plant Mol. Biol.* **53**, 715–731 (2003).
16. M. Ito, A. Koike, N. Koizumi, H. Sano, *Plant Physiol.* **133**, 1747–1754 (2003).
17. S. B. Preuss *et al.*, *Mol. Cell* **32**, 673–684 (2008).
18. J. A. Law, S. E. Jacobsen, *Nat. Rev. Genet.* **11**, 204–220 (2010).
19. Y. Liu, X. Zhang, R. M. Blumenthal, X. Cheng, *Trends Biochem. Sci.* **38**, 177–183 (2013).
20. H. W. Gabel *et al.*, *Nature* **522**, 89–93 (2015).
21. A. Bartlett *et al.*, *Nat. Protoc.* **12**, 1659–1672 (2017).
22. H. Stroud, M. V. C. Greenberg, S. Feng, Y. V. Bernatavichute, S. E. Jacobsen, *Cell* **152**, 352–364 (2013).
23. M. E. Potok *et al.*, *Nat. Commun.* **10**, 3352 (2019).
24. W. J. J. Soppe *et al.*, *Mol. Cell* **6**, 791–802 (2000).
25. H. Stroud *et al.*, *Nat. Struct. Mol. Biol.* **21**, 64–72 (2014).
26. A. Finka, R. U. H. Mattoo, P. Goloubinoff, *Cell Stress Chaperones* **16**, 15–31 (2011).
27. V. B. V. Rajan, P. D'Silva, *Funct. Integr. Genomics* **9**, 433–446 (2009).
28. Q. Q. Zhao, R. N. Lin, L. Li, S. Chen, X. J. He, *J. Integr. Plant Biol.* **61**, 120–139 (2019).
29. L. M. Johnson *et al.*, *Nature* **507**, 124–128 (2014).
30. J. Gallego-Bartolomé *et al.*, *Cell* **176**, 1068–1082.e19 (2019).
31. L. Leng *et al.*, *J. Plant Res.* **130**, 349–363 (2017).
32. R. Rosenzweig, N. B. Nillegoda, M. P. Mayer, B. Bukau, *Nat. Rev. Mol. Cell Biol.* **20**, 665–680 (2019).

ACKNOWLEDGMENTS

We thank M. Akhavan and the Broad Stem Cell Research Center BioSequencing core for high-throughput sequencing; E. Ograg for help with plant care; C. Picard, Z. Zhong, and G. Barisano for bioinformatic scripts; V. Ramani, N. J. Abdulhay, and A. Keith for guidance with the EM-seq of in vitro methylated DNA; and B. Panning and members of the Jacobsen laboratory for helpful advice and discussions. **Funding:** This work was supported by NIH R35 GM130272 to S.E.J., the UCSF Program for Breakthrough Biomedical Research and the Sandler Foundation to S.R., NIH R01 GM089778 to J.A.W., NIH R35 GM134744 and CPRIT RR160029 to X.C. (who is a CPRIT Scholar in Cancer Research), NIH/NIGMS K99 GM135515 to S.H.D, the Philip Whitcome Pre-Doctoral Fellowship in Molecular Biology to L.I., and the Ruth L. Kirschstein National Research Service Award GM007185 to B.A.B.. S.E.J. is an investigator of the Howard Hughes Medical Institute. **Author contributions:** S.E.J. conceived and supervised the study. S.E.J.,

L.I., and C.J.H. designed the research. L.I. performed the experiments and analyzed the data. B.A.B performed the FP assays. L.S. performed the DNA curtain assays. C.J.H. and L.I. performed the DAP-seq experiments. G.K performed the structural modeling. M.A.G. and M.T. contributed to the in vivo experiments. S.F. performed the library preparation for total RNA-seq, GRO-seq, and BS-PCR. Y.J. performed the mass spectrometry. S.H.D performed the GRO-seq. J.A.W. supervised the mass spectrometry. X.C. supervised the structural modeling. S.R. supervised the DNA curtain assays. B.A.B, L.S, S.H.D, G.K., and Y.J. contributed to manuscript writing. L.I. and S.E.J. wrote the paper. **Competing interests:** The authors declare no competing interests. **Data and materials availability:** The high-throughput sequencing data generated in this paper have been deposited in the Gene Expression Omnibus (GEO) database (accession no. GSE165095).

SUPPLEMENTARY MATERIALS

science.sciencemag.org/content/372/6549/1434/suppl/DC1
Materials and Methods
Figs. S1 to S19
Table S1
References (*33*–*58*)
MDAR Reproducibility Checklist

View/request a protocol for this paper from *Bio-protocol*.

16 January 2021; accepted 20 May 2021
Published online 3 June 2021
10.1126/science.abg6130

MBD5 and MBD6 couple DNA methylation to gene silencing through the J-domain protein SILENZIO

Lucia Ichino, Brandon A. Boone, Luke Strauskulage, C. Jake Harris, Gundeep Kaur, Matthew A. Gladstone, Maverick Tan, Suhua Feng, Yasaman Jami-Alahmadi, Sascha H. Duttke, James A. Wohlschlegel, Xiaodong Cheng, Sy Redding and Steven E. Jacobsen

Science **372** (6549), 1434-1439.
DOI: 10.1126/science.abg6130originally published online June 3, 2021

Methyl readers that repress transcription

DNA methylation is a conserved epigenetic mark required for gene silencing in many different organisms. However, how the methyl mark is able to silence genes is still largely unknown. Ichino *et al.* discovered two *Arabidopsis* proteins named MBD5 and MBD6 that are recruited to DNA by direct recognition of methylation. These methyl readers recruit the class C J-domain protein SILENZIO to chromatin to silence methylated genes and transposons. SILENZIO likely acts through its interaction with heat shock chaperone proteins.

Science, abg6130, this issue p. 1434